Physica C 469 (2009) 566–574

Contents lists available at ScienceDirect

Physica C

journal homepage: www.elsevier.com/locate/physc

High-field phase-diagram of Fe arsenide superconductors

Y.J. Jo [a], J. Jaroszynski [a], A. Yamamoto [a], A. Gurevich [a], S.C. Riggs [a], G.S. Boebinger [a], D. Larbalestier [a], H.H. Wen [b], N.D. Zhigadlo [c], S. Katrych [c], Z. Bukowski [c], J. Karpinski [c], R.H. Liu [d], H. Chen [d], X.H. Chen [d], L. Balicas [a,*]

[a] National High Magnetic Field Laboratory, Florida State University, Tallahassee-FL 32310, USA
[b] Institute of Physics, Chinese Academy of Sciences, Beijing 100190, PR China
[c] Laboratory for Solid State Physics, ETH Zürich, CH-8093 Zürich, Switzerland
[d] Hefei National Laboratory for Physical Science a Microscale and Department of Physics, University of Science and Technology of China, Hefei, Anhui 230026, PR China

ARTICLE INFO

Article history:
Available online 19 March 2009

PACS:
74.25.–q
74.25.Ha
74.25.Op
74.70.Dd

Keywords:
High magnetic fields
Electrical transport
Torque magnetometry
Superconducting phase-diagram

ABSTRACT

Here, we report an overview of the phase-diagram of single-layered and double-layered Fe arsenide superconductors at high magnetic fields. Our systematic magneto-transport measurements of polycrystalline $SmFeAsO_{1-x}F_x$ at different doping levels confirm the upward curvature of the upper critical magnetic field $H_{c2}(T)$ as a function of temperature T defining the phase boundary between the superconducting and metallic states for crystallites with the ab planes oriented nearly perpendicular to the magnetic field. We further show from measurements on single-crystals that this feature, which was interpreted in terms of the existence of two superconducting gaps, is ubiquitous among both series of single- and double-layered compounds. In all compounds explored by us the zero temperature upper critical field $H_{c2}(0)$, estimated either through the Ginzburg–Landau or the Werthamer–Helfand–Hohenberg single gap theories, strongly surpasses the weak-coupling Pauli paramagnetic limiting field. This clearly indicates the strong-coupling nature of the superconducting state and the importance of magnetic correlations for these materials. Our measurements indicate that the superconducting anisotropy, as estimated through the ratio of the effective masses $\gamma = (m_c/m_{ab})^{1/2}$ for carriers moving along the *c*-axis and the *ab-planes*, respectively, is relatively modest as compared to the high-T_c cuprates, but it is temperature, field and even doping dependent. Finally, our preliminary estimations of the irreversibility field $H_m(T)$, separating the vortex-solid from the vortex-liquid phase in the single-layered compounds, indicates that it is well described by the melting of a vortex lattice in a moderately anisotropic uniaxial superconductor.

1. Introduction

The iron-based oxypnictides represent a novel class of superconductors which, with the exception of the cuprates, have the highest known superconducting transition temperature T_c [1,2]. Several series of these compounds have been synthesized in the last year, but throughout this manuscript we will mostly focus on the properties of the single-layered oxypnictide $LnFeAsO_{1-x}F_x$ (*Ln* is a lanthanide), or the so-called 1111 compounds, and on the $AEFe_2As_2$ (*AE* is an alkali-earth metal), or the so-called 122 compounds.

Both electric transport measurements and electronic band structure calculations suggest that undoped oxypnictides are semimetals [3]. There is an approximate nesting between the hole Fermi surface (FS) centered at the Γ point and the electron FS centered at the M point, which may lead to a spin-density wave (SDW) like instability state observed at low temperatures [4,5]. According to neutron diffraction studies, the magnetic structure of undoped pnictides is composed of antiferromagnetically coupled ferromagnetic chains [6]. Superconductivity in the 1111 or electron doped compounds would occur when part of the Fe^{2+} ions are replaced by Fe^{+}, which is expected to suppress the antiferromagnetic instability.

Several superconducting pairing mechanisms based on the multi-band nature of these compounds have been proposed. Dai et al. [7] suggested a spin-triplet pairing mechanism with even parity due to ferromagnetic spin fluctuations between electrons in different orbitals. Lee and Wen [8] argued that the strong Hunds rule ferromagnetic interaction in Fe pnictides can lead to a pairing instability in the spin-triplet *p*-wave channel in the weak-coupling limit, so that the superconducting gap would have nodal points on the two-dimensional Fermi surfaces. While Lee et al. suggested that because of the frustrating pairing interactions among the electron and the

* Corresponding author.
E-mail address: balicas@magnet.fsu.edu (L. Balicas).

0921-4534/$ - see front matter © 2009 Elsevier B.V. All rights reserved.
doi:10.1016/j.physc.2009.03.010

hole fermi-surface pockets, a $s + id$ pairing state with broken time reversal symmetry could be favored [9]. Perhaps, the model that is currently more widely accepted is the so-called extended $s^{\pm}$-wave model, which predicts a π shift between the order parameters on the hole and the electron Fermi-surface sheets [4]. In this scenario, the unconventional pairing mechanism is mediated by antiferromagnetic spin fluctuations. In fact, inelastic neutron scattering in the $Ba_{0.6}K_{0.4}Fe_2As_2$ compound reveals the emergence of a localized resonant magnetic excitation below the superconducting transition temperature [10]. This type of excitation is expected for a superconducting order parameter which has opposite signs in different parts of the Fermi surface as in the $s^{\pm}$ scenario. A general overview of the different pairing scenarios in oxypnictides is given by Mazin and Schmalian in this volume [11].

It is interesting to mention a recent photoemission report [12] claiming the existence of an underlying electronic (π,π) order in $Ba_{1-x}K_xFe_2As_2$, previously seen in the cuprates [13] and claimed to be perhaps at the origin of the observed small Fermi-surface pockets, as also seen in underdoped $YBa_2Cu_3O_{7+\delta}$ [14]. Thus the coexistence and non-trivial interplay of different order parameters seems to be an essential ingredient for high temperature superconductivity, in either the cuprates or the oxypnictides.

As for the existence of multiple superconducting gaps owing to the multi-band nature of the Fe arsenides the situation is still somewhat inconclusive. Several point contact spectroscopy studies yield contradictory results, with evidence for both single [15] and multi-gap superconductivity [16]. The latter does not invalidate the multi-band pairing scenario but rather indicates that the gaps of approximately equal magnitudes may reside on different disconnected sheets of the Fermi surface. At the same time, detailed local magnetization measurements via Hall probe magnetometry [17], photoemission [18,19] and neutron [10] measurements are consistent with a two-gap superconducting scenario for the 122 compounds.

The exact shape of the $H - T$ superconducting phase-diagram can help distinguish between different theoretical scenarios. Moreover, magneto-transport measurements under strong magnetic field can also determine the temperature dependence of the irreversibility field, which is one of the key parameters quantifying the potential of the oxypnictides for future power applications. However, it is already clear [20,21] that these compounds are characterized by tremendously large upper critical fields, requiring very high magnetic field techniques to explore the overall complexity of their superconducting phase-diagram. This is in turn a very encouraging result for applied superconductivity.

There have been already several reports on the physical properties of the Fe arsenides at very high magnetic fields. Two relevant reports, provide (i) evidence for two-gap superconductivity to explain the upward curvature of the upper critical field as a function of temperature for fields along the c-axis direction in 1111 compounds [20,21], and (ii) an evidence that the $H_{c2}(T)$ of the 122 compounds is weakly anisotropic despite the two-dimensional character of their Fermi surface, thus indicating that a strong anisotropy may not be instrumental for the high-T_c superconductivity in the Fe arsenides [22].

One of the greatest challenges at the moment is to achieve the synthesis of high quality single-crystals, and to explore their phase diagrams at very high fields not only by traditional magneto-tranport measurements but also by thermodynamic means. Here, we provide a brief overview of our initial efforts in this direction.

2. Experimental

Polycrystalline samples with nominal composition $SmFeAsO_{1-x}F_x$ were synthesized in Heifei by conventional solid state reaction using high-purity SmAs, SmF_3, Fe and Fe_2O_3 as starting materials. SmAs was obtained by reacting Sm chips and As pieces at 600 °C for 3 h and then 900 °C for 5 h. The raw materials were thoroughly ground and pressed into pellets. The pellets were wrapped in Ta foil, sealed in an evacuated quartz tube, and finally annealed at either 1160 °C or 1200 °C for 40 h. X-ray diffraction (XRD) pattern for a sample annealed at 1160 °C did reveal trace amounts of the impurity phase SmOF [2].

For the growth of $SmFeAsO_{1-x}F_x$ single-crystals at ETH [23], FeAs, Fe_2O_3, Fe and SmF_3 powders were used as starting materials and NaCl/KCl was used as flux. The precursor to flux ratio varied between 1:1 and 1:3. Pellets containing precursor and flux were placed in a BN crucible inside a pyrophyllite cube with a graphite heater. Six tungsten carbide anvils generated pressure on the whole assembly (3 GPa was applied at room temperature). While keeping pressure constant, the temperature was ramped up within 1 h to the maximum value of 1350–1450 °C, maintained for 4–10 h and decreased in 5–24 h to room temperature for the crystal growth. Then pressure was released, the sample removed and in the case of single-crystal growth NaCl/KCl flux was dissolved in water. Below, in our discussion concerning the irreversibility line in the 1111 compounds, we include some measurements previously reported by us in Ref. [21] in $NdFeAsO_{0.7}F_{0.3}$ single-crystals (see Ref. [24] for the details concerning the sample synthesis) which were originally used to extract the boundary between metallic and superconducting states at high fields.

The results reported here on 122 compounds were measured on single-crystals of $BaFe_{2-x}Co_xAs_2$ and $Ba_{1-x}K_xFe_2As_2$ grown at Hefei by the self-flux method. In order to avoid contamination from incorporation of other elements into the crystals, FeAs was chosen as self-flux. FeAs and CoAs powder was mixed together, then roughly grounded. The Ba pieces were added into the mixture. The total proportion of Ba:(2-xFeAs+xCoAs) is 1:4. For more details, see Ref. [25]. A similar procedure was used to synthesize single-crystals of $Ba_{1-x}K_xFe_2As_2$.

For electrical transport measurements, polycrystalline samples were cut into bar shaped pieces. Contacts for the standard four probe measurements were made by attaching gold wires with silver epoxy. Contacts in single-crystals were made by the focused-ion-beam technique as described in Ref. [24]. For the magnetic torque measurements a $SmFeAsO_{0.8}F_{0.2}$ single-crystal was attached to the tip of a piezo-resistive micro-cantilever which was itself placed in a rotator inserted into a vacuum can. Changes in the resistance of the micro-cantilever associated with its deflection and thus a finite magnetic torque τ was measured via a Wheatstone resistance bridge. The ensemble was placed into a ^{4}He cryostat coupled to a resistive 35 T dc magnet. For the transport measurements we used a combination of pulsed and continuous fields including the 45 T hybrid magnet of the National High Magnetic Field Lab in Tallahassee.

3. Results and discussion

3.1. Polycrystalline material

In Fig. 1 we show typical resistivity curves for polycrystalline $SmFeAsO_{1-x}F_x$ as a function of temperature under several values of magnetic field and for four nominal doping levels, $x = 0.1$, 0.15, 0.18, and 0.2, [26] respectively. The first striking feature is that one does not see a very pronounced broadening of the superconducting transition under strong fields, in marked contrast with the thermally-activated broadening seen in the cuprates [27]. Although, both polycrystalline and single crystalline $SmFeAsO_{1-x}F_x$ samples exhibit clear signatures for thermally-activated flux-flow [21] indicating the existence of a vortex-liquid state over a broad range of temperatures and magnetic fields. The broad peak seen in the resistivity above the superconducting state for $x = 0.1$

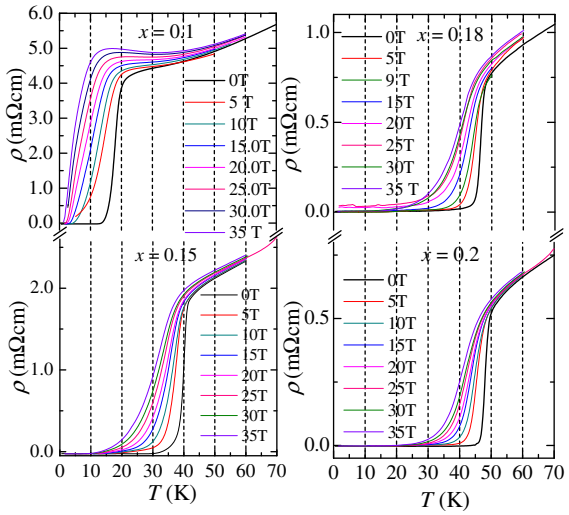

Fig. 1. Resistivity of $SmFeAsO_{1-x}F_x$ as a function of temperature for several magnetic field values and for four doping levels $x = 0.1$, 0.15, 0.18 and 0.2.

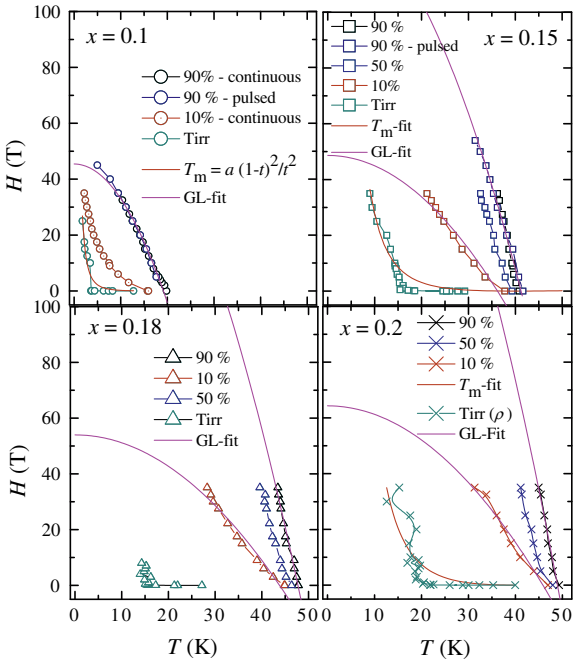

Fig. 2. The superconducting phase-diagram of polycrystalline $SmFeAsO_{1-x}F_x$ for the four doping levels shown in Fig. 1. Black and dark blue points represent the position of the onset (90%), blue points represent middle point (50%) while red points represent the foot (10%) of the resistive transition. Magenta lines are fits to the expression $H_c = H_{c2}(0)[1-t^2]$ while red lines are attempts to describe onset of the zero resistance state (green markers) through an anisotropic vortex melting line, $T_m = a\frac{(1-t)^2}{t^2}$, where $t = T/T_c$. (For interpretation of the references to color in this figure legend, the reader is referred to the web version of this article).

results from a remarkable magnetoresistive effect observed only in the under-doped compounds, i.e. $x < 0.15$, a behavior previously reported by us in Ref. [28] where we drew a comparison with the under-doped cuprates. In this case, the onset of the resistive transition under field was defined as 90% of the value of the resistivity maximum in the normal state just above the transition.

The conventional way of analyzing the resistive transition in a polycrystalline layered material like $SmFeAsO_{1-x}F_x$ is to assume that the onset of the superconducting transition is dominated by those crystallites with the ab planes oriented nearly along the magnetic field direction. In turn, the bottom of the resistive transition (at which the resistivity $\rho(T,H)$ drops below 10% of its normal-state value ρ_n) would be dominated by either those crystallites with the *ab*-plane oriented perpendicular to the magnetic field or by the melting of the vortex lattice, as has been observed in the cuprates. Thus, by measuring the temperatures of the onset and the foot of the resistive transition under field, one can infer the the temperature dependencies of the upper critical fields H_{c2} for both field orientations. But a word of caution is needed here. For polycrystalline material the width of the superconducting transition under field is affected by several factors including vortex fluctuations and the coupling strength between the grains. Thus, the foot of the transition in polycrystalline material may not reflect the actual behavior of H^c_{c2} for fields applied along the inter-plane direction if the Ginzburg parameter is of the order of 10^{-2} like in YBCO [21]. In 122 compounds and in the La based 1111 compounds the fluctuation Ginzburg parameter Gi is of the order of 10^{-4} indicating that vortex fluctuations are not that important, and the foot of the resistive transition does reflect the true behavior of $H^c_{c2}(T)$ [20]. The situation becomes more complicated in Nd and Sm 1111 compounds, for which Gi is of the same order as in YBCO [21]. Nevertheless, as we will see below, there is a qualitative agreement between the behavior of H^c_{c2} estimated for polycrystalline material, and the behavior of H^c_{c2} measured in single-crystals where it can be defined as a true onset of superconductivity at 90% or 99% of the normal-state resistivity for the corresponding field orientation.

Fig. 2 shows the respective phase diagrams for the different doping levels displayed in Fig. 1. [1]Dark blue symbols correspond to the onset of the superconducting transition (corresponding to 90% of the resistivity of the normal state just prior to the resistive transition), blue markers depict the midpoint of the transition, while red ones correspond to the foot the superconducting transition defined as $\rho(T,H) = 0.1\rho_n$. Green markers indicate the position in field and temperature where the resistivity of our samples drops below our experimental sensitivity. These points could reflect the behavior of the irreversibility field if one could neglect inter- or intra-granularity effects which are relevant for polycrystalline material. As we will see below, this "irreversibility field" obtained in this way behaves very differently from the melting field H_m measured in single-crystals. Furthermore, as is clearly seen in Fig. 2, these points move very quickly to low temperatures as small fields are applied, which would either suggest an extreme two-dimensionality (which contradicts the observed anisotropy in H_{c2} and in the ρ for these materials) or strong granularity effects.

Two important aspects can be clearly seen from the data: (i) the extrapolation of the upper critical fields to zero temperature $H_{c2}(0)$ estimated either from the slope of $H_{c2}(T)|_{T\to T_c}$ through the Werthamer–Helfand–Hohenberg expression or through the simple phenomenological expression $H_{c2}(T) = H_{c2}(0)(1-(T/T_c)^2)$ yields $H_{c2}(0)$ values which are several times larger than k_BT_c/μ_B, particularly for in-plane fields (for example, for $x = 0.2$ one has $T_c \simeq 48$ K while $H^{ab}_{c2}(0)$ obtained for the onset of the SC transition from both methods yields, respectively, $H^{ab}_{c2}(0) = (247 \pm 17)$ T and (221 ± 15) T) and (ii) the position of the foot of the resistive transition which is expected to represent the upper critical field $H^c_{c2}(T)$ along the *c*-axis shows an upward curvature or a nearly divergent behavior as the temperature is lowered. Observation (i) may be indicative of unconventional superconductivity and perhaps strong-coupling pairing or even for a prominent role for the spin–orbit interaction, since the values for $H_{c2}(0)$ quoted above are several times larger than the the weak-coupling Pauli limiting field, $H_p[T]$

[1] For interpretation of color in Figs. 1, 2, 3, 4 and 9, the reader is referred to the web version of this article.

$\simeq 1.84 k_B T_c[K]$. The observation (ii) has been interpreted in terms of a two-gap superconducting pairing [20], in line with the extended *s*-wave model [4]. As was first pointed out by Ref. [29], polycrystalline 1111 materials exhibit an appropriate scaling, which enable us to collapse all the graphs in Fig. 2, i.e. all the superconducting phase diagrams for the different doping levels, in a single diagram as shown in Fig. 3a. Here, the points correspond, respectively, to the onset, middle point and foot of the resistive transitions under field normalized with respect to the square of their values for the superconducting transition temperature (T_c^2) at each doping, and as functions of the reduced temperature $t = T/T_c$. This scaling has a simple explanation based on the small size of the coherence lengths in oxypnictides. The in-plane and the inter-plane upper critical fields, $H_{c2}^{ab}(T) \simeq \phi_0/2\pi\xi_{ab}(T)\xi_c(T)$ and $H_{c2}^{c}(T) \simeq \phi_0/2\pi\xi_{ab}^2(T)$ (ϕ_0 is the magnetic flux quantum), are determined by the respective out-of-plane and in-plane coherence lengths $\xi_c = \xi_{ab}\gamma^{-1/2}$ where $\gamma = m_c/m_{ab}$ is the effective mass anisotropy parameter. In a *clean* limit for which the mean free path $\ell$is much greater than ξ at $T \ll T_c$, the coherence lengths scale like T_c^{-1}, leading naturally to $H_{c2} \propto T_c^2$. In other words, as argued in Ref. [29], despite the presence of impurity phases, as discussed in the previous section, and the granularity inherent to a polycrystalline material, the coherence lengths in this material are small enough for the Cooper pairs not to be significantly affected by the impurities, grain size or inter-grain coupling. There are two main differences between this graph and a similar one shown in Ref. [29] (i) it extends this scaling over a broad range in $t = T/T_c$, where the upward curvature of H_{c2}^{c} becomes quite evident and (ii) H_{c2}^{ab} or the onset of the resistive transition also seems to satisfy the scaling. It further suggests that $H_{c2}^{ab}(0) \sim 0.13T_c^2$, which for a maximum $T_c = 55$ K would lead to $H_{c2}^{ab}(T=0) \sim 393$ T or nearly four times the value expected for H_p. However, one should keep in mind that the extrapolation of H_{c2} measured near T_c to lower temperatures following Ginzburg–Landau theory, disregards the essential paramagnetic limitations and could overestimate the actual $H_{c2}(0)$ values [21].

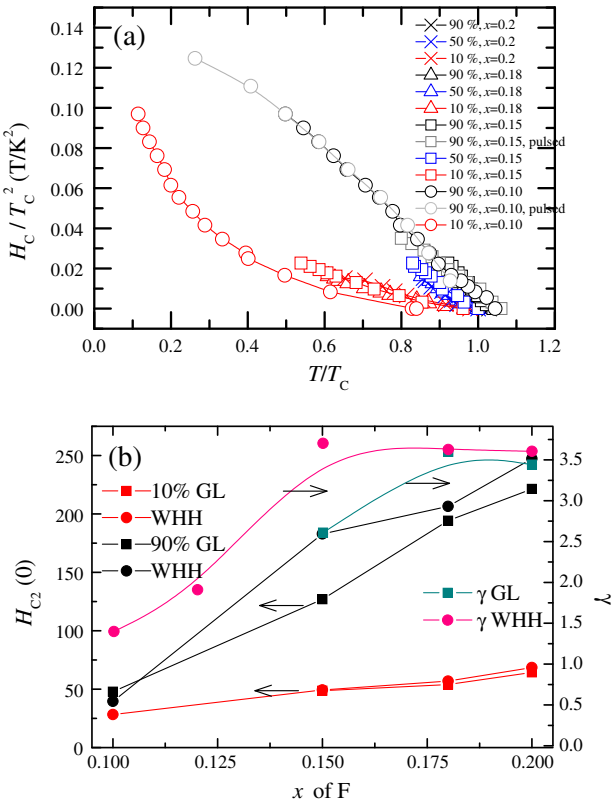

Fig. 3. Top panel: Renormalized superconducting phase-diagram of the $SmFeAsO_{1-x}F_x$ series. Despite the known existence of sub-phases in polycrystalline material, the observed scaling indicates that one is dealing with a material that is effectively in the clean limit. Bottom Panel: Estimations of the upper critical field at zero temperature $H_{c2}(0)$ from the WHH formulae (solid circles) and from the fit to $H_c = H_{c2}(0)[1\text{-}t^2]$ (solid squares). Red and black markers correspond to fits to points describing the *H-T* position of respectively the 10% ($\sim H_{c2}^{c}$) and 90% ($\sim H_{c2}^{ab}$) of the resistive transition. In the same graph we plot the anisotropy $\gamma = H_{c2}^{ab}/H_{c2}^{c}$ resulting from each fit. γ is seen to increase with F content saturating at a value of $\simeq$3.5. (For interpretation of the references to color in this figure legend, the reader is referred to the web version of this article).

Fig. 3b shows H_{c2}^{c} (red markers) and H_{c2}^{ab} (black markers) as extracted from the WHH formula, i.e $H_{c2}(0) \simeq -0.69\partial H_{c2}(T)/\partial T|_{T\to T_c} T_c$ (squares) and from the phenomenological equation $H_{c2}(T) \simeq H_{c2}(0)(1-(T/T_c)^2)$ (circles) as a function of the fluorine doping level *x*. It also shows the anisotropy $\gamma = H_{c2}^{ab}/H_{c2}^{c}$ obtained from both forms of estimating $H_{c2}(0)$. Both estimations suggest that γ increases with F content saturating at a value ~3.5. It is nevertheless quite unexpected that one is able to find such a scaling relation when the anisotropy is changing with the doping content. It is actually even more remarkable given the fact that this relation does not hold in double-layered single-crystals, which one would expect to be cleaner, as we will discuss below.

3.2. Single-crystals of single-layered compounds

The high T_c values and the extremely high upper critical fields of the oxypnictides [20] could make them promising candidates for power applications if, unlike the layered cuprates, a sizeable vortex liquid region responsible for dissipative flux-flow does not dominate a large portion of their temperature–magnetic field (*T–H*) phase-diagram. Therefore it is important to study the response of the anisotropic magnetization in the vortex state of the oxypnictides, in particular, the extent to which vortex properties are affected by strong magnetic correlations, multi-band effects and a possible interband phase shift between order parameters on the different sheets of the Fermi surface. For instance, multi-band effects are known to manifest themselves in MgB_2 as a strong temperature and field dependency of the mass anisotropy parameter $\gamma(T,H)$ and of the London penetration depth $\lambda(T,H)$ even at $H \ll H_{c2}$ [31,32].

Measurements of the anisotropic equilibrium magnetization $m(T,H)$ in 1111 single-crystals are complicated by the smallness of $m(H,T)$ caused by the large Ginzburg–Landau parameter, $\kappa = \lambda/\xi >$ 100 and by the strong paramagnetic response of the lanthanide and Fe ions, which can mask the true behavior of $m(T,H)$. In this situation torque magnetometry is the most sensitive technique to measure fundamental anisotropic parameters in $\mathbf{m}(T,H)$ particularly in small single-crystals. The torque $\tau = \mathbf{m} \times \mathbf{H}$ acting upon a uniaxial superconductor is given by [33,34]

$$\tau(\theta) = \frac{HV\phi_0(\gamma^2-1)\sin 2\theta}{16\pi\mu_0\lambda_{ab}^2\gamma\varepsilon(\theta)} \ln\left[\frac{\eta H_{c2}^{ab}}{\varepsilon(\theta)H}\right] + \tau_m \sin 2\theta, \quad (1)$$

where *V* is the sample volume, ϕ_0 is the flux quantum, H_{c2}^{ab} is the upper critical field along the ab planes, $\eta \sim 1$ accounts for the structure of the vortex core, θ is the angle between **H** and the *c*-axis, $\varepsilon(\theta) = (\sin^2\theta + \gamma^2\cos^2\theta)^{1/2}$ and $\gamma = \lambda_c/\lambda_{ab}$ is the ratio of the London penetration depths along the *c*-axis and the *ab*-plane. The first term in Eq. (1) was derived by Kogan in the London approximation valid at $H_{c1} \ll H \ll H_{c2}$ [33]. The last term in Eq. (1) describes the torque due to the paramagnetism of the lanthanide oxide layers and possible intrinsic magnetism of the FeAs layers. Here, $\tau_m = (\chi_c - \chi_a)VH^2/2$ and χ_c and χ_a are the normal-state magnetic susceptibilities of a uniaxial crystal along the c axis and the ab plane, respectively.

As we showed recently [35], the paramagnetic term in Eq. (1) in $SmO_{0.8}F_{0.2}FeAs$ single-crystals with $T_c \sim 45$ K can be larger than

the superconducting torque, which makes extraction of the equilibrium vortex magnetization rather non-trivial. This problem was circumvented by applying a simple mathematical procedure, which enabled us to unambiguously extract the superconducting component of the torque from the data by fitting the sum $\tau_{av}(\theta) + \tau_{av}(\theta + 90°)$, in which the odd harmonics due to the paramagnetic component cancel out:

$$\tau(\theta) + \tau(\theta + 90^\circ) = \frac{V\phi_0(\gamma^2 - 1)H \sin 2\theta}{16\pi\mu_0\lambda_{ab}^2\gamma} \times \left[\frac{1}{\varepsilon(\theta)} \ln\left(\frac{\eta H_{c2}^{\parallel}}{\varepsilon(\theta)H}\right) - \frac{1}{\varepsilon^{\star}(\theta)} \ln\left(\frac{\eta H_{c2}^{\parallel}}{\varepsilon^{\star}(\theta)H}\right)\right], \quad (2)$$

where $\varepsilon^{\star}(\theta) = (\cos^2\theta + \gamma^2 \sin^2\theta)^{1/2}$ and $\eta \simeq 1$.

The above discussion is illustrated by Fig. 4. For instance, Fig. 4a shows $\tau(\theta)$ for a $SmO_{0.8}F_{0.2}FeAs$ single crystal in a limited angular range and for both increasing and decreasing angular sweeps at $T = 27$ K and $H = 3$ T. The reversible component $\tau_{av}(\theta)$ is extracted by taking the average of both ascending and descending branches of $\tau(\theta)$. This procedure gives a characteristic behavior of $\tau_{av}(\theta)$ almost perfectly described by Eq. (1) represented by the red line. The fit yields a value $\gamma \simeq 11.5$ and a value for $H_{c2}^{ab} = \gamma H_{c2}^{c}$ that is considerably lower than the value extracted from our polycrystalline samples having a similar T_c (shown in Fig. 5b). The reason is that the direct three parameter fit using Eq. (1) is not very stable, allowing many different fit parameters to give equally good description of the torque data.

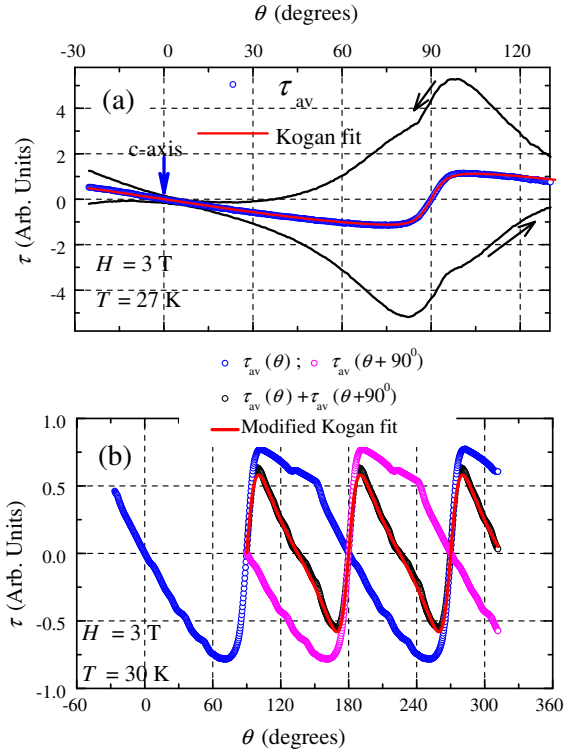

Fig. 4. (a) Magnetic torque $\tau(\theta)$ for a $SmOFeAs_{0.8}F_{0.2}$ single crystal for increasing and decreasing angle sweeps (black lines) at 3 T and 27 K. The reversible equilibrium $\tau_{av}(\theta)$ (blue markers) is obtained by averaging both traces. Red line is a fit to the Kogan expression from which one can extract the anisotropy parameter γ, in-plane penetration depth λ_{ab}, and inter-plane upper critical field H_{c2}^{c}, see text. (b) Angular dependence of $\tau_{av}(\theta)$ (blue) and $\tau_{av}(\theta + 90°)$ (magenta) for 3 T and 30 K. Such a procedure described in Ref. [35] suppresses the magnetic component in the torque associated to Sm or Fe ions. Red line corresponds to a fit of $\tau_{av}(\theta) + \tau_{av}(\theta + 90°)$ to a modified Kogan expression. (For interpretation of the references to color in this figure legend, the reader is referred to the web version of this article).

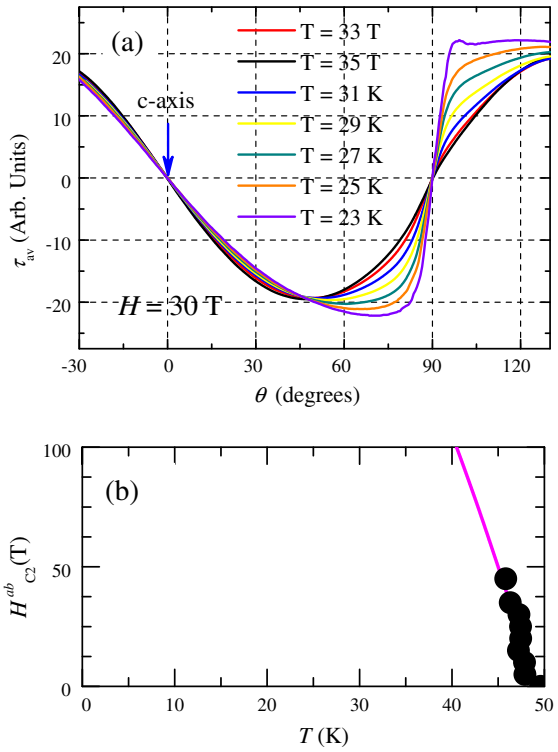

Fig. 5. (a) Angular dependence of $\tau_{av}(\theta)$ at 30 T and for several temperatures. (b) H_{c2}^{ab} from the resistive transition in polycrystalline $SmFeAsO_{0.82}F_{0.18}$ (black markers) and fit to the expression $H_c^{ab}(T) = H_c^{ab}(0)[1 - (T/T_c)^2]$ and which was used as input in Eq. (2). For all our fittings $\eta = 1$.

As mentioned above, the paramagnetic torque component $\tau_m \propto H^2$ becomes particularly pronounced at very high fields for which it can become larger than the equilibrium superconducting torque $\tau_s \propto Hln(H_{c2}/H)$. As a result, the application of the procedure based on Eq. (2) becomes the only way to unambiguously extract the relatively small component τ_s from the torque data. This is illustrated by Fig. 4b which shows $\tau_{av}(\theta)$, $\tau_{av}(\theta + 90°)$ and $\tau_{av}(\theta) + \tau_{av}(\theta + 90°)$, as a function of θ for $H = 3$ T and $T = 30$ K. As follows from Fig. 4b, the component of the torque due solely to the superconducting response shows a sharper and less "rounded" angular dependence. The important aspect is that this procedure not only gives a smaller value for $\gamma = 8.7$ but it also leads to an H_{c2}^{c} value, which is more consistent with our transport measurements in polycrystalline material. Although a word of caution is needed here. In multi-band superconductors, as is possibly the case for the oxypnictide superconductors, the superconducting anisotropy as extracted from the ratio of penetration depths may differ considerably from the anisotropy as extracted from the ratio of the upper critical fields. The Kogan formalism was developed assuming a single band scenario although it was latter extended to include possible differences among both anisotropies [34]. Given the lack of a proper multi-band formalism to analyze our torque data, our current strategy is to extract H_{c2}^{c} and H_{c2}^{ab} from transport measurements in our single-crystals, introduce both H_{c2}^{c} and the anisotropy ratio in H_{c2} within the extended Kogan formula [34] re-fitting our original data to extract the anisotropy in penetration depth, after subtraction of the paramagnetic component. Following our work, a similar strategy was already applied by Ref. [37]. This would avoid discrepancies in H_{c2}^{c} extracted from the transport and the torque data and among the values of H_{c2}^{c} extracted from different torque data sets, these [35] and those of Ref. [36]. The ability to perform

transport measurements in these single-crystals was developed only very recently. We expect, nevertheless that our main broad conclusions concerning the qualitative dependence of the anisotropy in temperature and field will remain valid.

Fig. 5a shows a data set of $\tau_{av}(\theta)$ taken under $H = 30$ T and for several temperatures, for which we applied the procedure illustrated by Fig. 4b. As discussed in Ref. [35], our systematic study of $\tau_{av}(\theta)$ gives $\gamma(H,T)$, which exhibits the field and temperature dependencies similar to those previously seen in MgB_2, further supporting the two-gap scenario for the single-layered oxypnictides. For fields all the way up to 30 T, we could not detect any noticeable effect of the field on the in-plane penetration depth (or equivalently on the superfluid density) that would indicate the suppression of a superconducting gap in one of the bands. This is remarkable, since as seen in Fig. 5b 30 T is very close to the values of H_{c2}^c (open markers), extracted from two sets of torque data measured at, respectively, 3 and 30 T and in the temperature range between 25 and 30 K, and suggests strong-coupling superconductivity (perhaps two very strongly coupled gaps), or perhaps even an abrupt first order transition [38].

3.2.1. Evaluation of the irreversibility line

Using the torque magnetometry technique it is also possible to extract the irreversibility field $H_m(T)$ by sweeping the field up and down at a given temperature and measuring the hysteretic magnetization loop, $m = \Delta\tau(H)/H = H^{-1}(\tau(H_\uparrow) + \tau\ (H_\downarrow))/2$. The field at which the magnetization loop closes defines the irreversibility line $H_m(T)$ that separates pinned vortex vortex-solid and vortex-liquid states. Below the irreversibility field the torque measurement of the irreversible component of the magnetization $\Delta m(H) = \Delta\tau(H)/H$ enable us to use the Bean critical state model [39] to extract the critical current density of a superconductor, $J_c = k\Delta m(H)/R$, and the pinning force $\mathbf{F}_p(H) = \mathbf{J}_c(H) \times \mathbf{H}$ per unit volume where k is a constant that depends on the geometry of the sample and R is the dimension of the sample perpendicular to the field direction. Thus, we have $J_c(H) \propto \Delta\tau(H)/H$ and $F_p\ (H) \propto \Delta\tau(H)$. For conventional type-II superconductors, scaling laws for flux pinning proposed by Dew-Hughes [40] Campbell and Evetts [41] or by Kramer [42] can be written in a general form as $F \propto H_{c2}^m h^p (1-h)^q$, with $h = H/H_{c2}$. For high T_c-cuprates superconductors, similar phenomenological scaling relations have been used [43], but with a different definition of the reduced field, $h = H/H_{irr}$ so that the critical current vanishes at H_{irr}.

Fig. 6a shows raw torque normalized by the field data for a $SmOFeAs_{0.8}F_{0.2}$ single crystal as a function of field H applied nearly along the c-axis, or more precisely for an angle $\theta \simeq 5 \pm 1°$ between H and the c-axis of the crystal as measured via a Hall probe. A very strong hysteresis, i.e., the irreversible component in the $\tau(H)/H$, emerges as the temperature is lowered, from which we can estimate the overall behavior of F_p. In the cuprates the pinning force curves taken at different temperatures often collapse into a scaling relation $F_p/F_p^{max} \propto h^p(1-h)^q$ where F_p^{max} is the maximum pinning force, and $h = H/H_{irr}$ [44]. As follows from Fig. 6b, the resulting pinning curves for the oxypnictides also tend to collapse into an asymptotic behavior given by the expression $F_p/F_p^{max} \propto h^{1/2}(1-h)^2$, similar to that of the Kramer model [42] in which J_c is determined by shear depinning of the vortex lattice. Fig. 6b also shows the asymptotic behavior $F_p/F_p^{max} \propto h(1-h)$ characteristic of a dense array of strong core pinning centers in NbTi [45]. It is clear that $F_p/F_p^{max} \propto h^{1/2}(1-h)^2$ provides a much better description of our data, indicating that the field dependence of the pinning force in our $SmOFeAs_{0.8}F_{0.2}$ sample is more reminiscent of that of Nb_3Sn [46] and $YBa_2Cu_3O_{7-x}$ [44].

The irreversibility field H_{irr} extracted from the analysis described above exhibits the temperature dependence $H_{irr}(t) \propto (1-t)/t^\alpha$ with $\alpha \approx 1$ for $NdOFeAs_{0.7}F_{0.3}$, and $\alpha \approx 0.6$ for $SmOFeAs_{0.8}F_{0.2}$ (see Fig. 7b). Such behavior of $H_{irr}(T)$ is similar to that of the melting field of the vortex lattice in moderately anisotropic uniaxial superconductors, for which $H_m(t) \propto t^{-\alpha}(1-t)^\beta$ with $1 < \alpha < 2$, $1 < \beta < 2$ [47]. This temperature dependence along with the fact that H_{irr} lies noticeably below H_{c2} indicate that vortex fluctuations in 1111 oxypnictides are rather strong, consistent with the estimations of the Ginzburg number Gi, which characterizes fluctuations of the order parameter near T_c. As shown earlier [21,29], the value of $Gi \sim 10^{-2}$ for $NdOFeAs_{0.7}F_{0.3}$ and $SmOFeAs_{0.8}F_{0.2}$ is of the same order of magnitude as Gi for $YBa_2Cu_3O_{7-x}$.

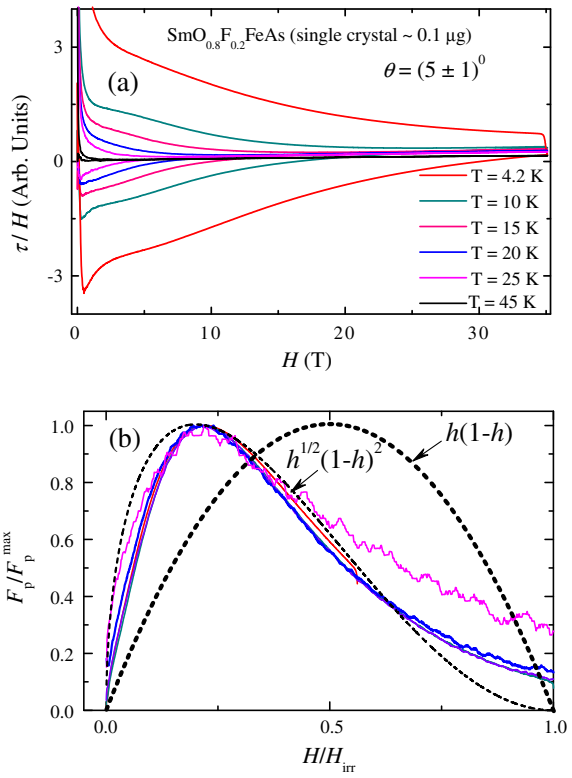

Fig. 6. (a) Magnetic torque τ normalized by the field H and as a function field for a $SmOFeAs_{0.8}F_{0.2}$ single crystal and for several temperatures. The vortex pinning force F_p is proportional the irreversible component in the torque, i.e., $\Delta\tau/H = H^{-1}[\tau(H_\uparrow) - \tau(H_\downarrow)$. (b) Pinning force F_p normalized with respect to its maximum value F_p^{max} as a function of the reduced field $h = H/H_{irr}$.

Significant vortex fluctuations in $NdOFeAs_{0.7}F_{0.3}$ single-crystals also manifest themselves in the clear Arrhenius plot of the resistance shown in Fig. 7a. This data that was already reported in Ref. [21], provide an unambiguous evidence for thermally-activated vortex dynamics in 1111 oxypnictides in a wide range of temperatures and fields. Our goal here is to evaluate H_{irr} from these transport measurements in order to compare it with H_{irr} extracted from our torque measurements in $SmOFeAs_{0.8}F_{0.2}$. For $NdOFeAs_{0.7}F_{0.3}$, which has a T_c close to the value reported for our $SmOFeAs_{0.8}F_{0.2}$ single crystal, we define the irreversibility field at which the resistivity drops below our experimental sensitivity (horizontal line in Fig. 7a). As follows from Fig. 7b, the agreement between our crude estimate from the transport data and the H_{irr} extracted from the torque data is quite remarkable, except perhaps for the points from the transport data at the highest fields which are subjected to a lower signal to noise ratio.

3.3. Single-crystals of double-layered compounds

In this section we present a detailed high-field magneto-transport study in the so-called double-layered or 122 Fe arsenide com-

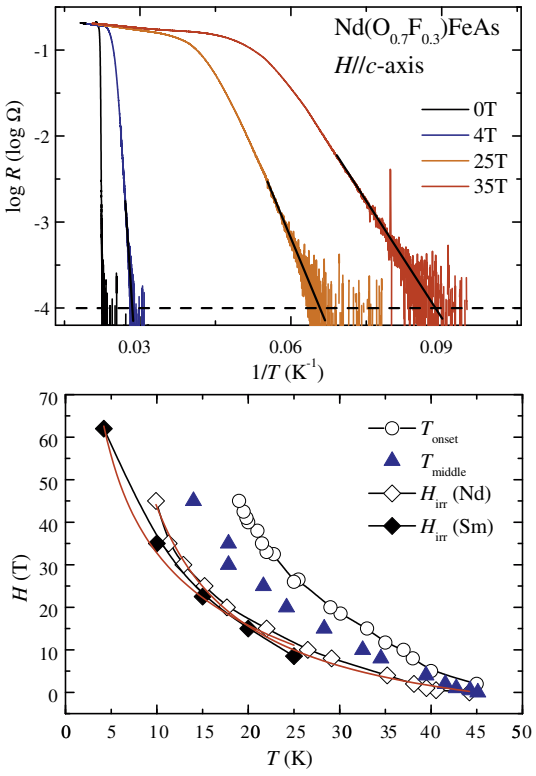

Fig. 7. Top panel: Logarithmic dependence of the resistive transition in a $NdOFeAs_{0.7}F_{0.3}$ single crystal as function of the inverse temperature T^{-1}, from Ref. [21]. The temperature at which the resistivity reaches the level of noise of our experimental set-up may reflect the behavior of the irreversibility line. Bottom panel: An attempt to draw the irreversibility line in the superconducting phase-diagram of the 1111 compounds from both transport and torque measurements. Circles and rectangles define respectively the onset and the middle point of the resistive transition in a $NdOFeAs_{0.7}F_{0.3}$ single crystal. Open rectangles depict the "irreversibility line" from transport measurements, while solid rectangles depict the irreversibility field extracted from our scaling analysis in Fig. 6 for $SmOFeAs_{0.8}F_{0.2}$. Red lines are fits to the expression $H_m(t) \propto t^{-\alpha}(1-t)$ with $1 < \alpha < 2$ (see text). (For interpretation of the references to color in this figure legend, the reader is referred to the web version of this article).

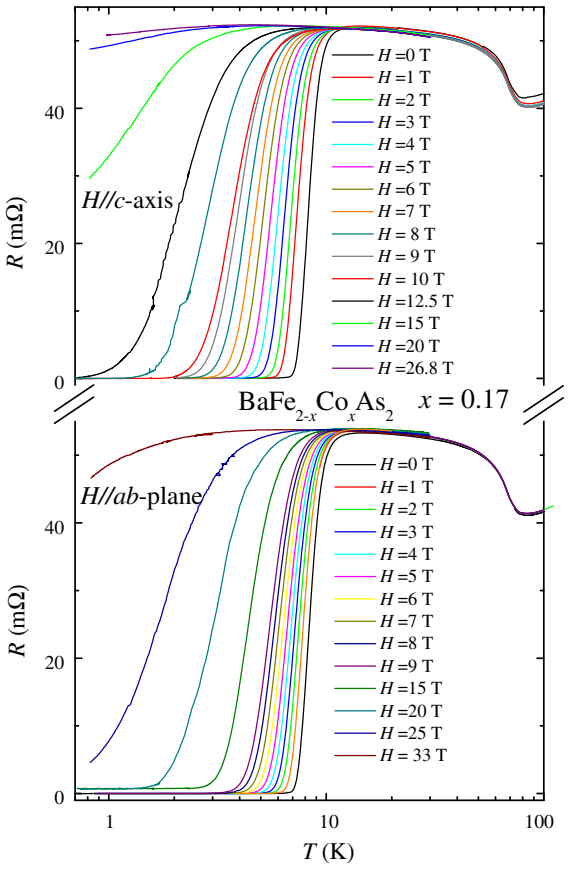

Fig. 8. (a) Resistance R as a function of temperature for a $BaFe_{2-x}Co_xAs_2$ single crystal having a nominal doping of 0.17 and for several field values oriented along an in-plane direction. (b) Same as in (a) but for fields along the inter-plane direction. The step observed at $T \sim 60$ K corresponds to the transition towards the antiferromagnetic state [51].

pounds with the goal of extracting their phase-diagram and drawing a comparison with the previously presented data on the 1111 compounds by addressing the following questions. Is the upward temperature dependence of $H_{c2}(T)$ along the c-axis a general feature of the Fe arsenide compounds? To what extent does a magnetic field broaden the phase-diagram of the 122 compounds as compared to that of the 1111s, or in other words, how similar is the vortex physics of the 122s with respect of that of the 1111s? Are the upper critical fields of these compounds at low temperatures as tremendously enhanced with respect to the weak-coupling Pauli limiting field as those of the 1111 compounds? Is there any possibility of observing new superconducting phases, such as the Fulde–Ferrel–Larkin–Ovchinnikov (FFLO) state [48] in these compounds? The search for answers to these questions was the motivating factor behind our preliminary exploration of the 122 compounds. Fig. 8a and b show a typical set of resistance data for a $BaFe_{1-x}Co_xAs_2$ single crystal (nominal doping $x = 0.17$) as a function of temperature for several field values and two field orientations along the c-axis and along the ab plane, respectively. Here, we show only data for a few samples whose superconducting transition width at zero field $\Delta T_c(H = 0) \lesssim 2$ K. In marked contrast with the 1111 compounds the width of superconducting transition is modestly affected by the external field, see for example similar data on Refs. [49,50]. Thus, the behavior of 122 compounds under field is much more akin to that of the low T_c superconducting compounds where the resistive transition does not broaden much but shifts to lower temperatures as a larger field is applied.

From several data sets like this we can come up with a superconducting phase-diagram for several 122 compounds shown in Fig. 9. It contains data for two nominal concentrations of $BaFe_{2-x}Co_xAs_2$, namely $x = 0.17$ and 0.18, and $Ba_{1-x}K_xFe_2As_2$ with a nominal concentration $x = 0.4$. The middle point of the resistive superconducting transition at zero field for each compound takes place at, $T = (8.1 \pm 0.1)$ K, (20 ± 0.05) K, and (28 ± 0.1) K, respectively. In Fig. 9 blue and red markers depict the superconducting phase boundary, respectively, for H parallel and perpendicular to the FeAs planes. Closed and open symbols depict respectively the onset (90%) and the foot or 10% of the normal-state resistivity.

The upward curvature seen in H_{c2} for $Ba_{0.6}K_{0.4}Fe_2As_2$ and for temperatures close to T_c may result from a distribution of superconducting transition temperatures, possibly due to a spread in the local doping levels. In this case our transport measurements of Hc2 defined at 90% of the normal-state resistivity mostly probe the superconducting properties of the regions with optimal doping for which T_c is maximum. It is interesting to compare our data with the heat capacity measurements of $H_{c2}(T)|_{T \to T_c}$ on the same material, which reveals a linear temperature dependence for $H_{c2}(T)$ [52]. Since the heat capacity measurements probe $H_{c2}(T)$ averaged over the entire distribution of T_cs, the difference between the transport and the specific heat measurements may reflect the difference in the temperature dependencies of $H_{c2}(T)$ in optimally doped and non-optimally doped regions.

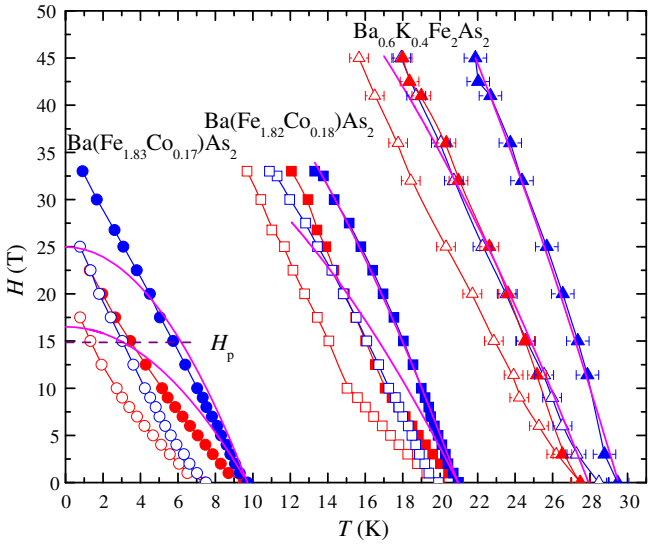

Fig. 9. Magnetic field H temperature T superconducting phase-diagram of several under-doped double-layered Fe arsenide compounds. Blue and red symbols depict the phase boundary for fields along an in-plane and the inter-plane directions, respectively. Closed and open symbols depict respectively the onset (90%) and the foot or 10% of the resistive transition. Triangles, squares and circles, represent the boundaries for $Ba_{0.6}K_{0.4}Fe_2As_2$, $BaFe_{1.82}Co_{0.18}As_2$, and $BaFe_{1.83}Co_{0.17}As_2$, respectively. Magenta lines are an attempt to the fit in each case the onset of the resistive transition to $H_{c2}(T) = H_{c2}(0)[1-(T/T_c)^2]$. For $Ba_{0.6}K_{0.4}Fe_2As_2$ we simultaneously measured two single-crystals with slightly different T_cs, one with the field oriented along the *ab*-plane and the other with the field applied along the *c*-axis. (For interpretation of the references to color in this figure legend, the reader is referred to the web version of this article).

Several important observations follow from the data shown in Fig. 9: (i) $H_{c2}(T)$ as a function of temperature for $H\|c$ is also concave as it is for the 1111 compounds, (ii) while $H_{c2}(T)$ for $H\perp c$ behaves nearly linearly in temperature, at least as seen for the $BaFe_{1.83}Co_{0.17}As_2$ compound for which we were able to explore a larger portion of its superconducting phase-diagram, (iii) the upper critical fields extrapolated to zero temperature for both field orientations are clearly well beyond the week coupling Pauli limiting field, i.e. for $BaFe_{1.83}Co_{0.17}As_2$ one obtains $H_p = 1.84 \times 8.1 \simeq 14.9$ T. In reality, for fields applied along the *ab*-plane the extrapolation of H_{c2} to zero temperature gives values about twice the BCS paramagnetic limit. Notice, that for reasons that are currently unclear, the $H_{c2}(T)$ values found by us for $BaFe_{2-x}Co_xAs_2$ are considerably larger than the ones reported in Ref. [49] for samples having approximately the same T_cs. Our observations immediately suggest a parallelism with strongly coupled superconductors such as the heavy-fermion compounds. For example, in the so-called 115 compounds the ratio $2\Delta_0/k_BT_c$ is claimed to be much larger than the BCS value 1.76 [53] while $H_{c2}(T)$ along an in-plane direction extrapolated to zero temperature surpasses by far the expected weak-coupling Pauli limiting field [54]. It has also been argued, at least for the Co doped compounds, that there might be a finite although small spread in the local Co concentrations in different parts of the sample [49], thus creating an intrinsic disorder. Disorder could also contribute to the increase in the upper critical field in these materials [55,21]. In fact, the phase-diagrams of the 122 compounds shown in Fig. 9, do not follow the scaling shown in Fig. 1 for the 1111 compounds, indicating that these nominally single-phase single-crystals may not be in the clean limit. It is interesting to mention, for instance, that a simple fit of the onset of $H_{c2}(T)$ for $Ba_{0.6}K_{0.4}Fe_2As_2$ for fields along the planar direction to the expression $H_{c2}(T) = H_{c2}(0)(1-(T/T_c)^2)$ (magenta lines in Fig. 9) yields $H_{c2}(0) = (100 \pm 2)$ T, which is a factor of 2 higher than H_p. Although, as we have learned from $BaFe_{1.83}Co_{0.17}As_2$ this expression may strongly underestimate $H_{c2}(0)$. In all three cases, the anisotropy $\gamma = H^{ab}_{c2}(T)/H^{c}_{c2}(T)$ is observed to decrease from a value $\gamma \gtrsim 3$ for $T \to T_c$ to a value $\gamma \gtrsim 1$ for $T \ll T_c$ as already reported in Ref. [22].

4. Conclusions

In conclusion in all oxypnictide compounds explored by us we observe:

1. A pronounced upward curvature in the temperature dependencies of $H_{c2}(T)$ along the *c*-axis.
2. Relatively modest effective mass anisotropies which are temperature dependent (as seen in MgB_2), reaching values in the order of 9 at low temperatures for the 1111 compounds or values ranging between 3 and 1 (at low temperatures and high fields) for the 122 compounds
3. Upper critical fields extrapolated to zero temperature that are a factor of two to three higher than the weak-coupling Pauli limiting field as in the heavy-fermion compounds.

All points listed above are clear indications for unconventional superconductivity in the Fe arsenides: points 1 and 2 are consistent with a two-gap scenario [20,21], and point 3 may indicate a significant enhancement of the Pauli limiting field by strong-coupling effects. The more anisotropic single-layered 1111 compounds, which display the highest T_cs in the oxypnictide family, exhibit a field-temperature superconducting phase-diagram similar to that of the least anisotropic cuprates. This manifests itself in the existence of a irreversibility field H_{irr} well below $H_{c2}(T)$, ohmic thermally-activated flux flow resistivity at $H_{irr}(T) < H < H_{c2}(T)$, and a temperature dependence for H_{irr} which is consistent with that of the melting field of the vortex lattice in a moderately anisotropic uniaxial superconductor. Yet despite the relatively strong vortex fluctuations in the 1111 compounds, their phase diagrams do not exhibit the very wide vortex liquid phase regions characteristic of layered Bi-2223 and Bi-2212 cuprates. In fact, as follows from Fig. 9, the irreversibility field H_{irr} above which 1111 compounds can carry weakly dissipative currents exceeds 30 T at 10 K, which is higher than $H_{irr}(T)$ for dirty MgB_2. These features of the oxypnictides (even in their present and far from optimized condition) along with their extremely high H_{c2} values can make these materials new promising contenders for high-field power applications.

Acknowledgements

The NHMFL is supported by NSF through Grant No. NSF-DMR-0084173 and the state of Florida. L.B. acknowledges the NHMFL in-house research program and Y.J.J. acknowledges the NHMFL-Schuller program.

References

[1] See, for example H. Takahashi, K. Igawa, K. Arii, Y. Kamihara, M. Hirano, H. Hosono, Nature 453 (2008) 376;
G.F. Chen, Z. Li, D. Wu, G. Li, W.Z. Hu, J. Dong, P. Zheng, J.L. Luo, N.L. Wang, Phys. Rev. Lett. 100 (2008) 247002.
[2] X.H. Chen, T. Wu, G. Wu, R.H. Liu, H. Chen, D.F. Fang, Nature 453 (2008) 761.
[3] S. Lebègue, Phys. Rev. B 75 (2007) 035110;
D.J. Singh, M.H. Du, Phys. Rev. Lett. 100 (2008) 237003;
G. Xu, W. Ming, Y. Yao, X. Dai, S.-C. Zhang, Z. Fang, Europhys. Lett. 82 (2008) 67002.
[4] I.I. Mazin D.J. Singh, M.D. Johannes, M.H. Du, Phys. Rev. Lett. 101 (2008) 057003.
[5] J. Dong, H.J. Zhang, G. Xu, Z. Li, G. Li, W.Z. Hu, D. Wu, G.F. Chen, X. Dai, J.L. Luo, Z. Fang, N.L. Wang, Europhys. Lett. 83 (2008) 27006.
[6] Clarina de la Cruz, Q. Huang, J.W. Lynn, Jiying Li, W. Ratcliff II, J.L. Zarestky, H.A. Mook, G.F. Chen, J.L. Luo, N.L. Wang, Pengcheng Dai, Nature 453 (2008) 899.
[7] Xi Dai, Zhong Fang, Yi Zhou, Fu-Chun Zhang, Phys. Rev. Lett. 101 (2008) 057008.
[8] Patrick A. Lee, Xiao-Gang Wen, 2008, arXiv:0804.1739.

[9] Wei-Cheng Lee, Shou-Cheng Zhang, Congjun Wu, 2008, arXiv:0810.0887.
[10] A.D. Christianson, E.A. Goremychkin, R. Osborn, S. Rozenkranz, M.D. Lumsden, C.D. Malliakas, I.S. Todrov, H. Klaus, D.Y. Chung, M.D. Kanatzidis, R.I. Bewley, T. Guidi, Nature 456 (2008) 930.
[11] I.I. Mazin, J. Schmalian, 2009, arXiv:0901.4790.
[12] V.B. Zabolotnyy, D.S. Inosov, D.V. Evtushinsky, A. Koitzsch, A.A. Kordyuk, G.L. Sun, J.T. Park, D. Haug, V. Hinkov, A.V. Boris, C.T. Lin, M. Knupfer, A.N. Yaresko, B. Büchner, A. Varykhalov, R. Follath, S.V. Borisenko, Nature 457 (2009) 569.
[13] E.M. Motoyama, G. Yu, I.M. Vishik, O.P. Vajk, P.K. Mang, M. Greven, Nature 445 (2007) 186.
[14] N. Doiron-Leyraud, C. Proust, D. LeBoeuf, J. Levallois, J.-B. Bonnemaison, R. Liang, D.A. Bonn, W.N. Hardy, L. Taillefer, Nature 447 (2007) 565.
[15] See for example T.Y. Chen, Z. Tesanovic, R.H. Liu, X.H. Chen, C.L. Chien, Nature 453 (2008) 1224.
[16] Y.L. Wang, L. Shan, L. Fang, P. Cheng, C. Ren, H.H. Wen, Supercond. Sci. Technol. 22 (2009) 015018;
P. Samuely, P. Szabo, Z. Pribulova, M.E. Tillman, S.L. Bud'ko, P.C. Canfield, Supercond. Sci. Technol. 22 (2009) 014003.
[17] Cong Ren., Zhao-sheng Wang, Hui-qian Luo, Huan Yang, Lei Shan, Hai-Hu Wen, 2008, arXiv:0808.0805.
[18] H. Ding, P. Richard, K. Nakayama, K. Sugawara, T. Arakane, Y. Sekiba, A. Takayama, S. Souma, T. Sato, T. Takahashi, Z. Wang, X. Dai, Z. Fang, G.F. Chen, J.L. Luo, N.L. Wang, Europhys. Lett. 83 (2008) 47001.
[19] P. Richards, T. sato, K. Nakayama, S. Souma, T. Takahashi, Y.-M. Xu, G.F. Chen, J.L. Luo, N.L. Wang, H. Ding, Phys. Rev. Lett. 102 (2009) 047003.
[20] F. Hunte, J. Jaroszynski, A. Gurevich, D.C. Larbalestier, R. Jin, A.S. Sefat, M.A. McGuire, B.C. Sales, D.K. Christen, D. Mandrus, Nature 453 (2008) 903.
[21] J. Jaroszynski, F. Hunte, L. Balicas, Youn-jung Jo, I. Raicevic, A. Gurevich, D.C. Larbalestier, F.F. Balakirev, L. Fang, P. Cheng, Y. Jia, H.H. Wen, Phys. Rev. B 78 (2008) 174523.
[22] H.Q. Yuan, J. Singleton, F.F. Balakirev, S.A. Baily, G.F. Chen, J.L. Luo, N.L. Wang, Nature 457 (2009) 565.
[23] N.D. Zhigadlo, S. Katrych, Z. Bukowski, S. Weyeneth, R. Puzniak, J. Karpinski, J. Phys-Condens. Mater. 34 (2008) 342202.
[24] Y. Jia, P. Cheng, L. Fang, H. Luo, H. Yang, C. Ren, L. Shan, C. Gu, H.H. Wen, Appl. Phys. Lett. 20 (2008) 032503.
[25] X.F. Wang, T. Wu, G. Wu, H. Chen, Y.L. Xie, J.J. Ying, Y.J. Yan, R.H. Liu, X.H. Chen, 2008, preprint arXiv:0806.2452v1.
[26] R.H. Liu, G. Wu, T. Wu, D.F. Fang, H. Chen, S.Y. Li, K. Liu, Y.L. Xie, X.F. Wang, R.L. Yang, L. Ding, C. He, D.L. Feng, X.H. Chen, Phys. Rev. Lett. 101 (2008) 087001.
[27] See, for example Yoichi Ando, G.S. Boebinger, A. Passner, N.L. Wang, C. Geibel, F. Steglich, Phys. Rev. Lett. 77 (1996) 2065;
D.L. Feng, X.H. Chen, Phys. Rev. Lett. 101 (2008) 087001.
[28] S.C. Riggs, J.B. Kemper, Y. Jo, Z. Stegen, L. Balicas, G.S. Boebinger, F.F. Balakirev, Albert Migliori, H. Chen, R.H. Liu, X.H. Chen, 2008, arXiv:0806.4011.
[29] J. Jaroszynski, Scott C. Riggs, F. Hunte, A. Gurevich, D.C. Larbalestier, G.S. Boebinger, F.F. Balakirev, Albert Migliori, Z.A. Ren, W. Lu, J. Yang, X.L. Shen, X.L. Dong, Z.X. Zhao, R. Jin, A.S. Sefat, M.A. McGuire, B.C. Sales, D.K. Christen, D. Mandrus, Phys. Rev. B 78 (2008) 064511.
[31] M. Angst et al., Phys. Rev. Lett. 88 (2002) 167004;
A.V. Sologubenko et al., Phys. Rev. B 65 (2002) 180505(R);
S.L. Bud'ko, P.C. Canfield, Phys. Rev. B 65 (2002) 212501.
[32] R. Cubitt et al., Phys. Rev. Lett. 91 (2003) 047002;
M. Angst et al., Phys. Rev. B 70 (2004) 224513.
[33] V.G. Kogan, Phys. Rev. B 24 (1981) 1572.
[34] V.G. Kogan, Phys. Rev. Lett. 89 (2002) 237005.
[35] L. Balicas, A. Gurevich, Y.J. Jo, J. Jaroszynski, D.C. Larbalestier, R.H. Liu, H. Chen, X. H. Chen, N.D. Zhigadlo, S. Katrych, Z. Bukowski, J. Karpinski, 2008, arXiv:0809.4223.
[36] S. Weyeneth, R. Puzniak, U. Mosele, N.D. Zhigadlo, S. Katrych, Z. Bukowski, J. Karpinski, S. Kohout, J. Roos, H. Keller, 2008, arXiv:0806.1024.
[37] S. Weyeneth, R. Puzniak, N.D. Zhigadlo,S. Katrych, Z. Bukowski, J. Karpinski, H. Keller, 2008, arXiv:0811.4047.
[38] V. Barzykin, L.P. Gor'kov, Phys. Rev. Lett. 98 (2007) 087004.
[39] For the original work see, for example C.P. Bean, Rev. Mod. Phys. 36 (1964) 31.
[40] D. Dew-Hughes, Philos. Mag. 30 (1974) 293.
[41] A.M. Campbell, J.E. Evetts, Adv. Phys. 21 (1972) 199.
[42] E.J. Kramer, J. Appl. Phys. 44 (1973) 1360.
[43] See, for example H. Yamasaki, K. Endo, S. Kosaka, M. Umeda, S. Yoshida, K. Karimura, Phys. Rev. Lett. 70 (1993) 3331.
[44] Z. Chen, D.M. Feldmann, X. Song, S.I. Kim, A. Gurevich, J.L. Reeves, Y.Y. Xie, V. Selvamanikam, D.C. Larbalestier, Supercond. Sci. Technol. 20 (2007) 205.
[45] C. Meingast, D.C. Larbalestier, J. Appl. Phys. 66 (1989) 5971.
[46] A. Godeke, B. ten Haken, H.H.J. ten Kate, D.C. Larbalestier, Supercond. Sci. Technol. 19 (2006) R100.
[47] G. Blatter, M.V. Feigel'man, V.B. Geshkenbein, A.I. Larkin, V.M. Vinokur, Rev. Mod. Phys. 66 (1994) 1125.
[48] See, for recent examples A. Bianchi, R. Movshovich, C. Capan, P.G. Pagliuso, J.L. Sarrao, Phys. Rev. Lett. 91 (2003) 187004;
H.A. Radovan, N.A. Fortune, T.P. Murphy, S.T. Hannahs, E.C. Palm, S.W. Tozer, D. Hall, Nature 425 (2003) 51;
M. Kenzelmann, Th. Strssle, C. Niedermayer, M. Sigrist, B. Padmanabhan, M. Zolliker, A.D. Bianchi, R. Movshovich, E.D. Bauer, J.L. Sarrao, J.D. Thompson, Science 321 (2008) 1652.
[49] N. Ni, M.E. Tillman, J.-Q. Yan, A. Kracher, S.T. Hannahs, S.L. Bud'ko, P.C. Canfield, Phys. Rev. B 78 (2008) 214515.
[50] A. Yamamoto, J. Jaroszynski, C. Tarantini, L. Balicas, J. Jiang, A. Gurevich, D.C. Larbalestier, R. Jin, A.S. Sefat, M.A. McGuire, B.C. Sales, D.K. Christen, D. Mandrus, Appl. Phys. Lett. 94 (2009) 062511.
[51] X.F. Wang, T. Wu, G. Wu, R.H. Liu, H. Chen, Y.L. Xie, X.H. Chen, 2008, arXiv:0811.2920.
[52] U. Welp, R. Xie, A.E. Koshelev, W.K. Kwok, H.Q. Luo, Z.S. Wang, G. Mu, H.H. Wen, 2008, arXiv:0810.1944.
[53] See, for example S. Kawasaki, M. Yashima, Y. Mugino, H. Mukuda, Y. Kitaoka, H. Shishido, Y. Onuki, Phys. Rev. Lett. 96 (2006) 147001.
[54] T.P. Murphy, Donavan Hall, E.C. Palm, S.W. Tozer, C. Petrovic, Z. Fisk, R.G. Goodrich, P.G. Pagliuso, J.L. Sarrao, J.D. Thompson, Phys. Rev. B 65 (2002) 100514(R).
[55] L.P. Gor'kov, Sov. Phys. JETP 17 (1963) 518.